CHAPTER 3

EXPERIMENTAL PROCEDURES

In this chapter, the experimental procedures employed for preparation and characterization of powders and ceramics in the (1-*x*)PZT–*x*doped BIT system (when x = 0, 0.1, 0.3, 0.5, 0.7, 0.9 and 1.0) will be described. Phase formation characterization has been carried out using X-ray diffraction (XRD). Microstructural was investigated by scanning electron microscopy (SEM). Electrical, ferroelectric properties and fatigue test were also characterized. The details are presented in the following sections.

3.1 Sample preparation

Fabrications of materials, including powder preparation (PZT, doped BIT and (1-*x*)PZT–*x*doped BIT) and ceramic fabrication ((1-*x*)PZT–*x*doped BIT) have been carried out follows.

3.1.1 Powder preparation

In this work, all powder compositions have been prepared by a solid-state mixed oxide method. All commercially available starting compounds which were used for the preparation of the compositions in this study are listed in Table 3.1, along with the suppliers, formula weights and purities.

Table 3.1 Specifications of the starting materials used in this study.

Powders	Source	Formula	Purity (%)
PbO	Fluka, Switzerland	223.20	99%
ZrO_2	Riedel-de Haën,	123.22	99%
TiO_2	Riedel-de Haën, German	79.89	99%
Bi_2O_3	Fluka, Switzerland	465.96	98%
Dy_2O_3	Cerac., Russia	372.99	99%
Nb_2O_5	Cerac., Russia	265.81	99%

3.1.1.1 Preparation of $Pb(Zr_{0.52}Ti_{0.48})O_3$ powder

In this work, the $Pb(Zr_{0.52}Ti_{0.48})O_3$ (PZT) powders were used as starting powders for all compositions of (1-*x*)PZT–*x*doped BIT systems. The PZT powder was first synthesized by a solid-state mixed oxide method. The following reaction was proposed for the formation of PZT powders:

$$PbO + 0.52ZrO_2 + 0.48TiO_2 \longrightarrow Pb(Zr_{0.52}Ti_{0.48})O_3 \quad (3.1)$$

The starting chemicals used were PbO, ZrO_2 and TiO_2. The powders were mixed by a ball-milling technique in distilled water for 24 hours and dried. A freeze-drying method was employed in order to dry powder. Freeze-drying involves of water or other solvent from a frozen product by a process called sublimation. Sublimation occurs when a frozen liquid goes directly to the gaseous state without passing through the liquid phase.

The freeze-drying process consists of three stages: prefreezing, primary drying and secondary drying. Firstly, prefreezing, the freezing is done rapidly, in order to lower the material to below its eutectic point quickly thus avoiding the formation of ice crystals. Usually, the freezing temperatures are between -40°C and -80°C. After

prefreezing the product, conditions must be established in which ice can be removed from the frozen product via sublimation, resulting in dry product. This process is called primary drying. In this phase, pressure is controlled through the application of partial vacuum. After primary freeze drying is complete and all ice has been sublimed, bound moisture is still present in the product. Continued drying is necessary at the warmer temperature to reduce the residual moisture content to optimum values. Then, the mixed powders were calcined at 800°C for dwell times 2 hours with a heating/cooling rate of 5°C/min in alumina crucible as shown in Figure 3.1. A schematic diagram of the PZT powder preparation is illustrated in Figure 3.2.

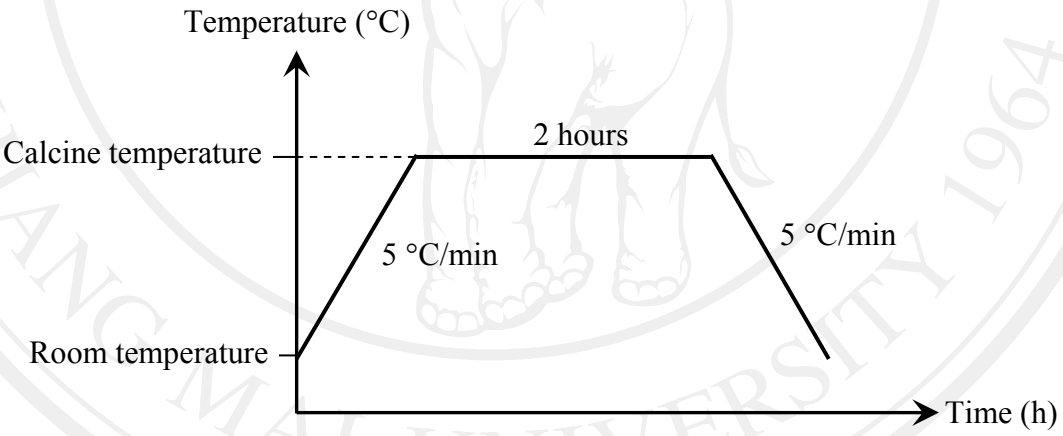

Figure 3.1 Diagram of calcination $Pb(Zr_{0.52}Ti_{0.48})O_3$ powder.

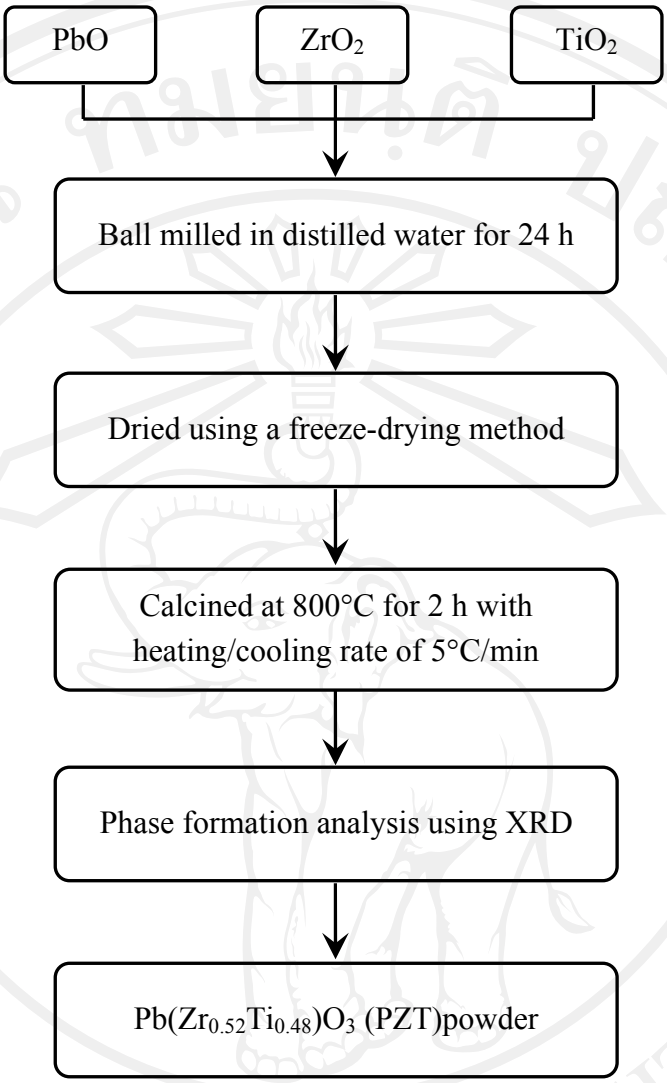

Figure 3.2 Diagram showing processing sequence of $Pb(Zr_{0.52}Ti_{0.48})O_3$ powders.

3.1.1.2 Preparation of $Bi_{3.25}Dy_{0.75}Ti_3O_{12}$ powder

The $Bi_{3.25}Dy_{0.75}Ti_3O_{12}$ with chemical formula $Bi_{4-x}Dy_xTi_3O_{12}$ (x = 0.75) powders were prepared by a solid-state mixed oxide method. The starting chemicals used were Bi_2O_3, TiO_2 and Dy_2O_3. The following reaction was proposed for the formation of BDT powders:

$$13Bi_2O_3 + 24TiO_2 + 3Dy_2O_3 \longrightarrow 8(Bi_{3.25}Dy_{0.75})Ti_3O_{12} \qquad (3.2)$$

The starting powders were weighted, ball-milled and dried. The mixed powders were calcined at various temperatures: 600, 650, 700, 750, 800, 850 and 900°C, for dwell time 4 hours with a heating/cooling rate of 5°C/min in an alumina crucible. Figure 3.3 shows the calcination process of powders. The X-ray diffraction analysis was employed to identify the phase formation in order to optimize the calcination temperature for the formation of BDT powder. Figure 3.4 shows processing sequence of BDT powder.

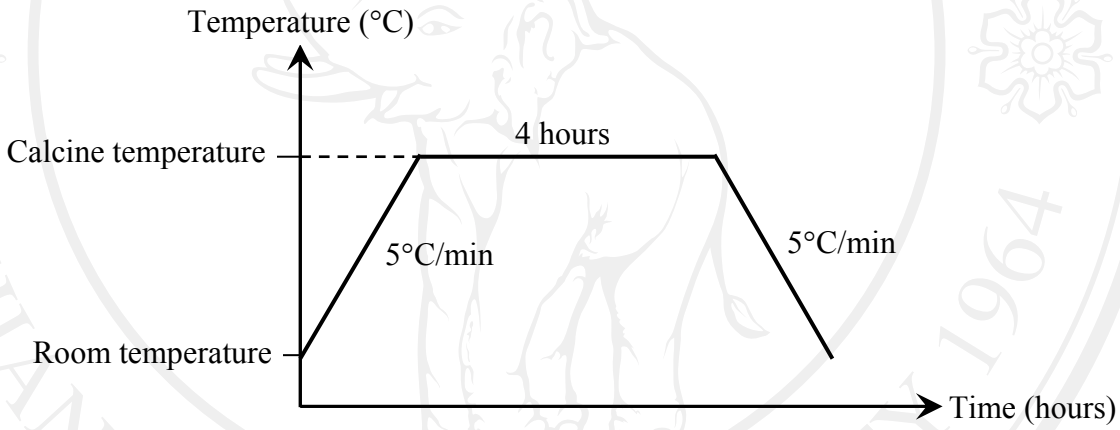

Figure 3.3 Diagram of calcination $Bi_{3.25}Dy_{0.75}Ti_3O_{12}$ and $Bi_{3.99}Ti_{2.97}Nb_{0.03}O_{12}$ powder.

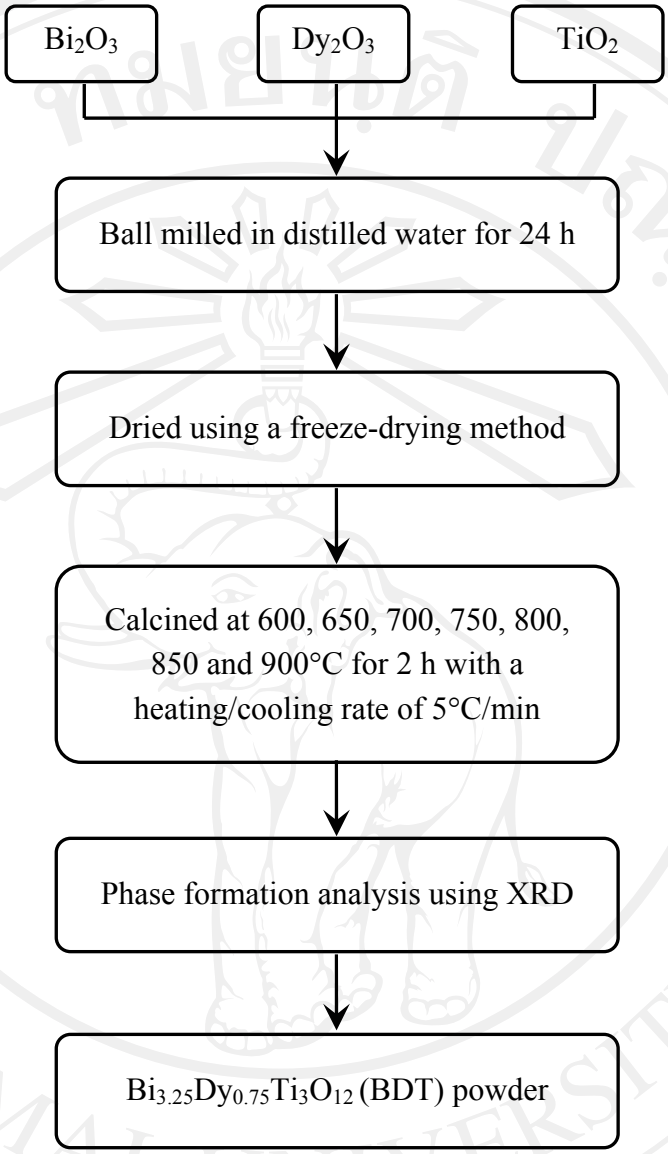

Figure 3.4 Diagram showing processing sequence of $Bi_{3.25}Dy_{0.75}Ti_3O_{12}$ powder.

3.1.1.3 Preparation of $Bi_{3.99}Ti_{2.97}Nb_{0.03}O_{12}$ powder

The $Bi_{3.99}Ti_{2.97}Nb_{0.03}O_{12}$ (BNbT) with chemical formula $Bi_{4-x/3}Ti_{3-x}Nb_xO_{12}$ (x = 0.03) powders were prepared by a solid state mixed-oxide method. The starting chemicals used were Bi_2O_3, TiO_2 and Nb_2O_5. The following reaction was proposed for the formation of BNbT powders:

$$1.995Bi_2O_3 + 2.97TiO_2 + 0.015Nb_2O_5 \longrightarrow Bi_{3.99}Ti_{2.97}Nb_{0.03}O_{12} \quad (3.3)$$

The starting powders were weighted, ball-milled and dried. The mixed powders were calcined at different temperatures which were 600, 650, 700, 750, 800, 850 and 900°C for dwell time 4 hours with a heating/cooling rate of 5°C/min in an alumina crucible. Figure 3.3 shows the calcination process of powders. The X-ray diffraction analysis was employed to identify the phase formation in order to optimize the calcination temperature for the formation of BNbT powder. The processing of powders is shown in Figure 3.5.

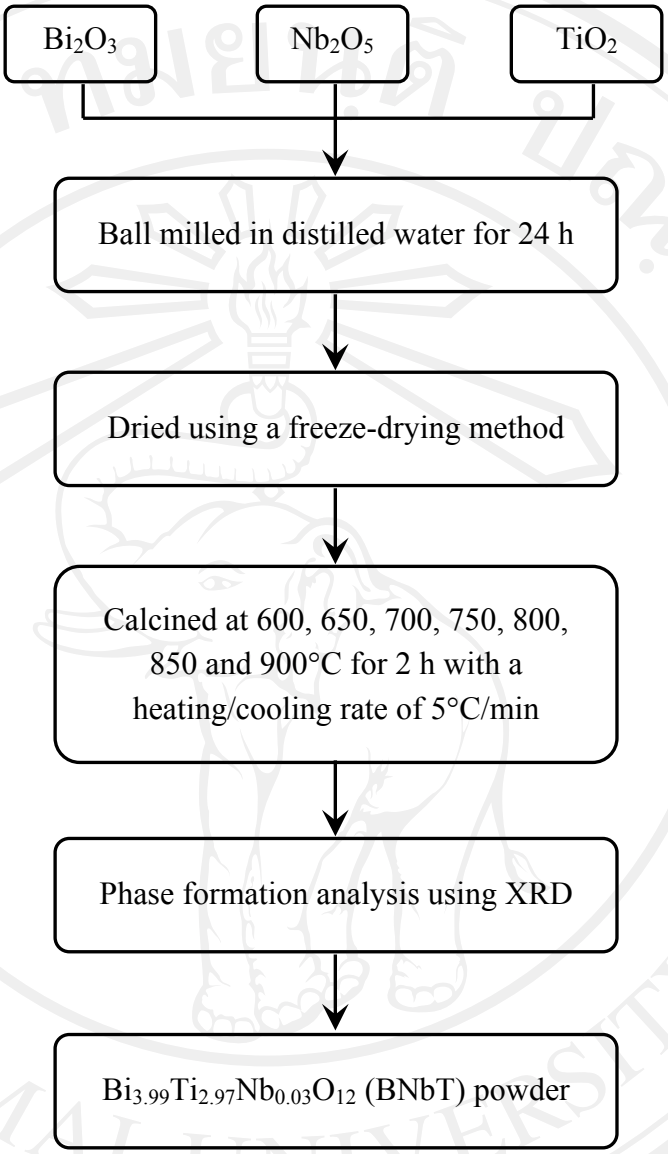

Figure 3.5 Diagram showing processing sequence of $Bi_{3.99}Ti_{2.97}Nb_{0.03}O_{12}$ powder.

3.1.1.4 Preparation of (1-*x*)PZT–*x*doped BIT powders

The mixed powders of high purity PZT and doped BIT ($Bi_{3.25}Dy_{0.75}Ti_3O_{12}$ and $Bi_{3.99}Ti_{2.97}Nb_{0.03}O_{12}$) were calcined at 800°C for 2 hours and at 900°C for 4 hours with a heating/cooling rate 5°C/min, respectively. The calcined powders of PZT and doped BIT (BDT and BNbT) were weighted, ball-milled and dried to produce the powder mixture of (1-*x*)PZT–*x*doped BIT, where *x* was the weight fraction and had

the values of 0, 0.1, 0.3, 0.5, 0.7, 0.9 and 1.0. The whole processing sequence for the preparation of (1-*x*)PZT–*x*doped BIT powders are shown in Figure 3.6.

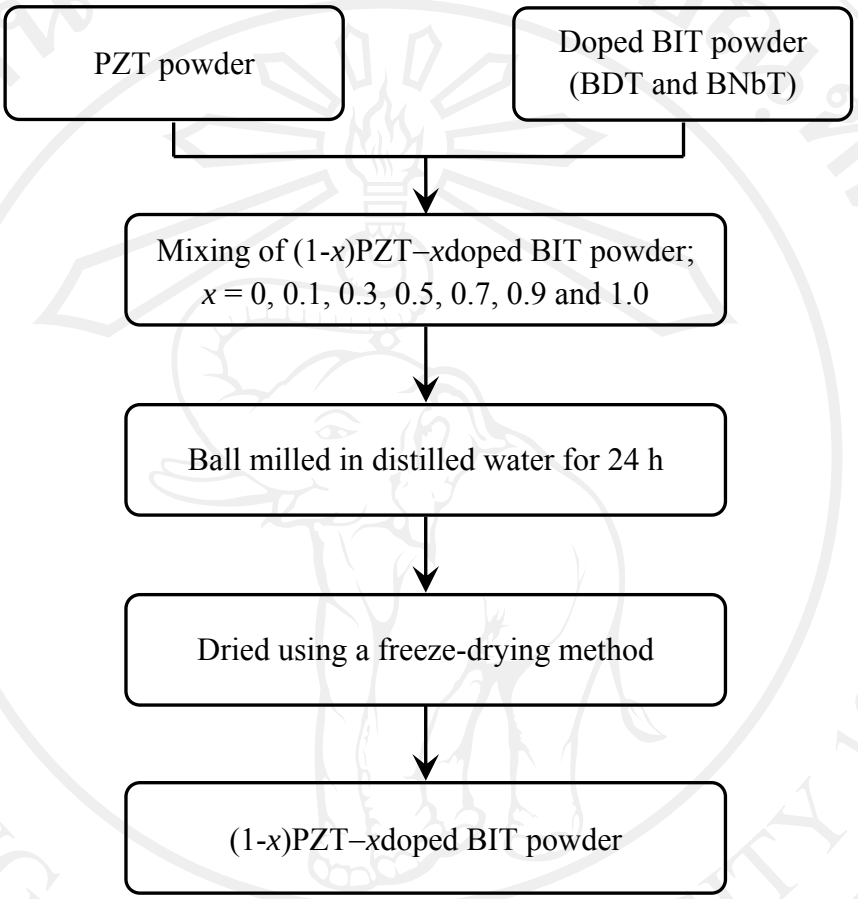

Figure 3.6 Diagram showing processing sequence of (1-*x*)PZT–*x*doped BIT powders.

3.1.2 Ceramic preparation

3.1.2.1 Preparation of (1-*x*)PZT–*x*BDT ceramics

After mixing the (1-*x*)PZT–*x*BDT powders, the mixed powders of each composition were uniaxial pressed (0.8 g per batch) of each composition into a green pellet with a diameter of 10 mm and a thickness of 1 mm, with 3 wt% polyvinyl alcohol (PVA) added as a binder. Following binder burn out at 500°C, the pellets

were placed on the alumina powder inside alumina crucible. In order to reduce loss of volatile components, e.g. lead and bismuth, the samples were covered with their own powders. The specimen arrangement is shown in Figure 3.7. The pellets were sintered at various sintering temperatures of 950, 1000, 1050 and 1100°C in air for dwell time 4 hours with a heating/cooling rate 5°C/min, sintering process as shown in Figure 3.8. The whole processing sequence for the preparation of (1-*x*)PZT−*x*doped BIT ceramics are shown in Figure 3.9.

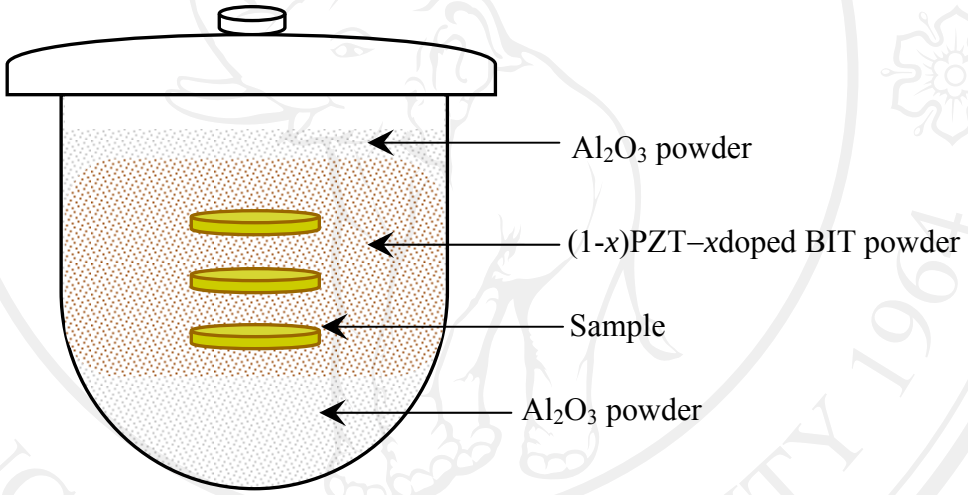

Figure 3.7 Sample arrangements for the sintering process.

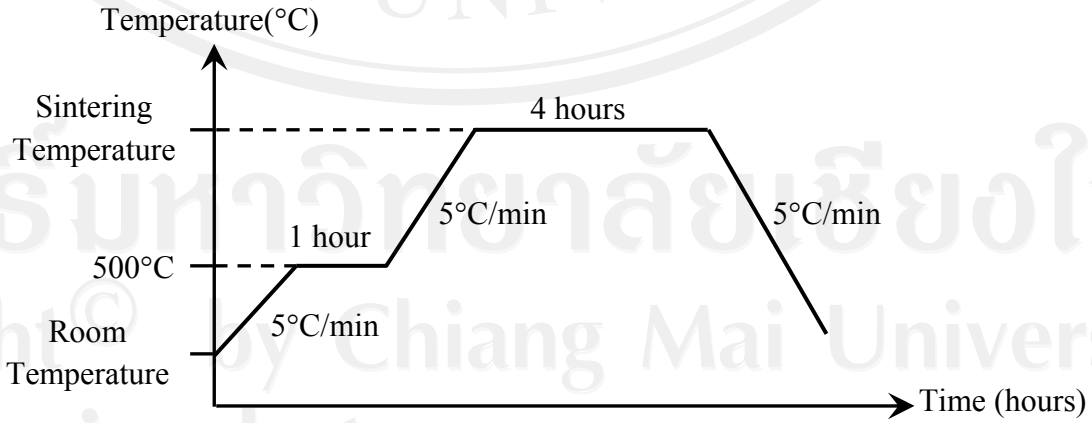

Figure 3.8 Diagram for sintering process.

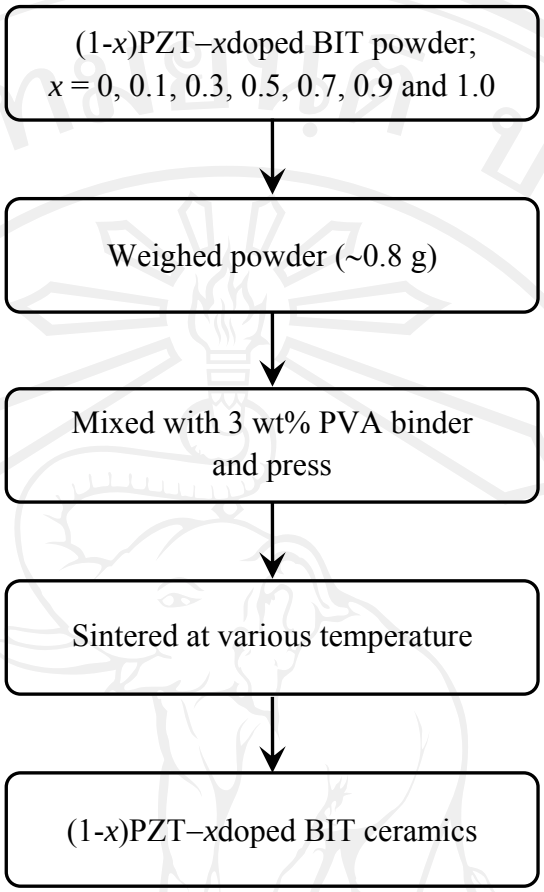

Figure 3.9 Diagram showing processing sequence of (1-*x*)PZT–*x*doped BIT ceramics.

3.2 Sample characterization

Characterization techniques used for subsequent investigation of phase formation, microstructures, dielectric and ferroelectric properties are described in following section.

3.2.1 X-ray diffraction (XRD)

In this study, the optimum firing temperatures, phase analysis of mixed powders and sintered ceramics were carried out using an X-ray diffractometer (XRD); Phillips Model X-pert (Figure 3.10). The source of X-ray employed CuKα radiation of wavelength 1.5405 Å, with a tube voltage and current of 40 kV and 35 mA,

respectively. Room temperature XRD data was recorded between 2θ range from 10° and 60° with a step size of 0.02°/second. The XRD database of ICSD was used to determine the phase formation of the samples.

Figure 3.10 X-ray diffractometer (Model Phillips Expert).

The X-ray beam incident on a material is partly scattered, absorbed and transmitted. The scattering of X-ray is related to the interaction between X-ray and crystal lattice of the materials. The X-ray scattered from different lattices interfere with each other and produces a diffraction pattern upon the change of incident angle of the X-ray beam. The X-ray reflectivity measurement configuration consist of the incident beam impinging on the sample material on a flat substrate and the X-ray reflected at the same angle as the incident radiation being detected. Peak detected

intensity will appear when Bragg's Law is satisfied as shown in Figure 3.11, which the equation is:

$$2d\sin\theta = n\lambda \tag{3.4}$$

where d is the interplanar spacing of the crystal,

θ is the angle of an incidence,

n is the integer order of the diffraction peak,

λ is the wavelength of the radiation (1.5405 Å).

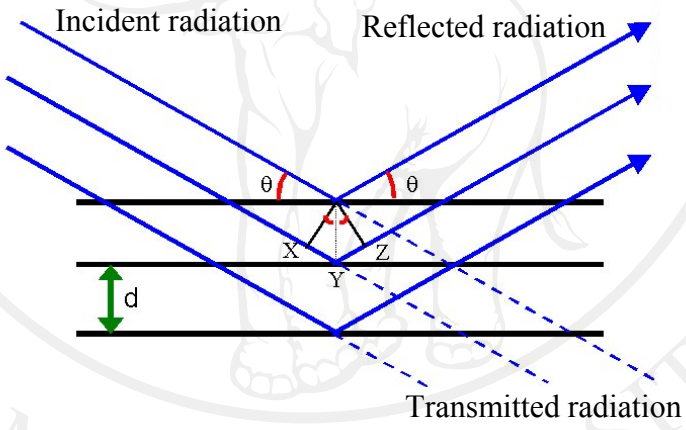

Figure 3.11 Schematic diagram of Bragg's law reflection.

3.2.2 Densification measurement

In this study, the bulk densities of sintered ceramics were determined using the Archimedes' principle. The sample is first weighed dry (W_1), then weighed again after fluid impregnation (W_2), and finally weighed while being immersed in fluid (W_3). The density (ρ) can be calculated from the following equation:

$$\rho = \frac{\rho_w w_1}{w_3 - w_2} \tag{3.5}$$

where ρ_w is the density of water (in g/cm^3), which is slightly temperature dependent,

$$\rho_w = 1.0017 - 0.0002315\ T \tag{3.6}$$

where T is the temperature of water (°C).

3.2.3 Scanning electron microscopy (SEM)

In this work, the scanning electron microscope (SEM, JEOL JSM-6335F) as shown in Figure 3.12, was used to determine the morphology of the surface and fracture toughness of the ceramics. The samples were polished and thermally etched at temperature 150°C lower than the sintering temperature with a heating/cooling rate of 5°C/min for dwell times 10 minutes. The thermal etched surface and fracture surface of the ceramics were cleaned by ultrasonic cleaner and coated with gold sputtering (shown in Figure 3.13). During image acquisition, secondary electron modes were used with an accelerating voltage of 15 kV. The range of grain size and average grain size were determined by using the linear intercept method to the SEM micrographs.

Figure 3.12 Scanning electron microscope (SEM, JEOL JSM-6335F).

Figure 3.13 Sputter coater (JFC-1100E).

3.2.4 Dielectric measurement

For dielectric measurement, the sintered samples were lapped to obtain parallel faces, which were subsequently coated with silver paint as electrodes. Then, the samples were tested with digital multimeter to check the quality of the electrodes. The dielectric properties were studied with an automated dielectric measurement system, LCZ-meter (Hewlett Packard 4194A) as shown in Figure 3.14. The capacitance and the dielectric loss tangent were determined at room temperature with the frequency 10 kHz. Therefore, the dielectric constant (ε_r) was then calculated by the following equation:

$$\varepsilon_r = \frac{Cd}{\varepsilon_0 A} \tag{3.7}$$

where C is the capacitance of the sample (F),

ε_0 is the dielectric permittivity of vacuum (8.854×10^{-12} F/m),

A is the area of the electrode of the sample (m^2),

d is the thickness of the sample (m).

Figure 3.14 The dielectric properties measurement at room temperature.

3.2.5 Ferroelectric measurement

The ferroelectric hysteresis (*P-E*) loops were characterized using a computer controlled modified Sawyer-Tower circuit. The electric field was applied to a sample by a high voltage AC amplifier (Trek 610D) with the input sinusoidal signal at fixed measuring frequency of 50 Hz from a function generator (GAG-809). The *P-E* loops were recorded by a digital oscilloscope (HP 54645A), as shown in Figure 3.15. The system is an automated device intended primarily for measuring the polarization of materials induced by an electric field. From each measurement, the samples were then placed inside the sample holder, which submerged in a silicone oil bath to prevent the breakdown of the sample and then connected to the standard capacitor on Sawyer-Tower circuit. The sample could be considered as a capacitor (C_s) connected in series to the standard capacitor (C_0). Since the capacitance of the sample was much smaller than that of the standard capacitor, almost all of the electric potential of the high voltage source acts on the sample.

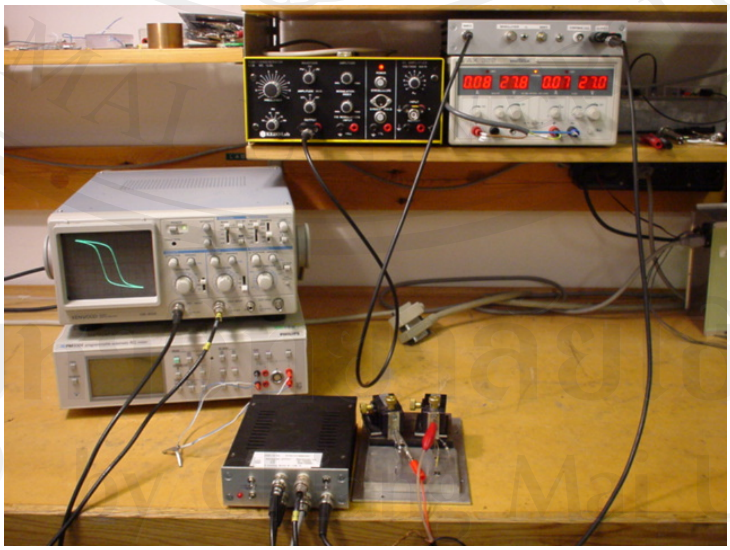

Figure 3.15 Ferroelectric hysteresis loop measurement.

By definition, polarization is the value of dipole moment per unit volume or amount of charge accumulated per unit surface area. Polarization of the sample induced by electric field loading, P_{sample} was given by

$$P_{sample} = \frac{Q_s}{A} \tag{3.8}$$

where Q_s is the amount of charges accumulated on the electrode of the sample (C),

A is the area of the electrode of the sample (cm^2).

Since the reference capacitor was connected in series to the sample, then amount of charges are equivalent:

$$Q_s = Q_0 \tag{3.9}$$

where Q_0 is the amount of charges accumulated on the standard capacitor (C).

On the other hand, the amount of charges on the standard capacitor is equal to:

$$Q_0 = V_y C_0 \tag{3.10}$$

where V_y is the voltage across the standard capacitor (V),

C_0 is the capacitance of the standard capacitor (= 1 μF).

Then, the polarization induced by electric field loading could be calculated as the following equation:

$$P_{sample} = \frac{V_y C_0}{A} \tag{3.11}$$

Consequently, by monitoring the voltage across the standard capacitor, the polarization of the sample could be determined.

From the *x*-axis of the monitor of oscilloscope, the electric field was calculated using the following equation:

$$E = \frac{V_x}{d} \tag{3.12}$$

where E is the electric field applied to the sample (V/cm),

V_x is the voltage across the circuit (V),

d is the thickness of the sample (cm).

3.2.6 Fatigue measurement

In ferroelectric materials, the direction of polarization switch can cause the damage evolution in the material [98, 99]. It implies the characteristics of the material decay. When the material is damaged, the shapes of its hysteresis loop changes (as shown in Figure 3.16). This damage is called fatigue behavior. Fatigue rate is defined as change in remanent polarization as a function of number of switching cycles. The remanent polarization (P_r) can be selected to examine the characteristics of fatigue behavior. The P_r is the polarization which appears when the applied electric field is

zero. For fatigue measurement, the loading conditions were obtained to sample. Therefore, the fatigue rate is affected by the loading conditions [67-83].

In this research, the loading conditions of fatigue measurement were fixed. The samples were fatigued under applied electric field of higher than 1.4 times the switching electric field (E_{sw}) [60, 100]. E_{sw} is defined as electric field which switching of polarization before breaks down with a frequency 50 Hz. The fatigue behavior was recorded up to 10^6 switching cycles. The remanent polarization (P_r) was computed from the recorded hysteresis loops. All the changes are given as normalized values represented as percentages of remanent polarization. During measurements, the samples were submerged in silicone oil, an insulating liquid to prevent arcing during fatigue process.

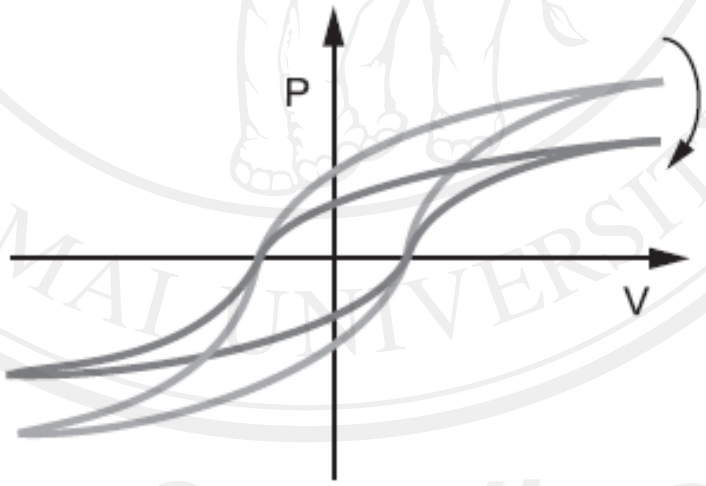

Figure 3.16 Polarization drop due to fatigue [101].

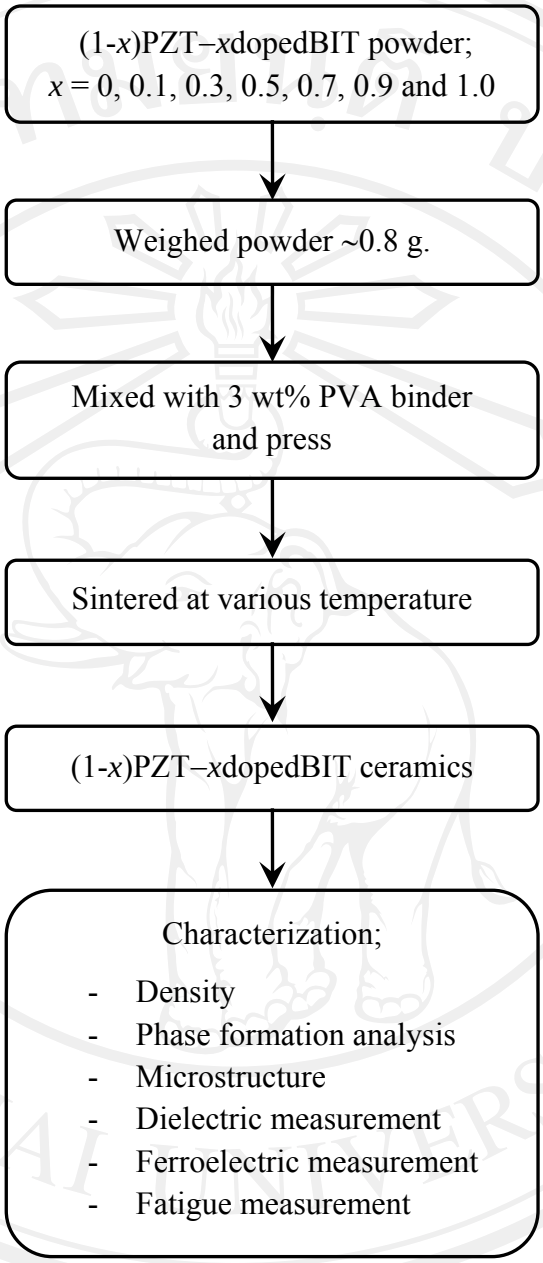

Figure 3.17 Diagram showing processing and characterization sequence of (1-*x*)PZT −*x*dopedBIT ceramics.